ISSN 1392–1320 MATERIALS SCIENCE (MEDŽIAGOTYRA). Vol. 16, No. 1. 2010

Kinetics of Growth and Sorption Properties of Evaporable Barium Getter Films

Audrius GIEDRAITIS[1*], Sigitas TAMULEVIČIUS[1,2], Rimantas GUDAITIS[2], Mindaugas ANDRULEVIČIUS[2]

[1]*Department of Physics, Kaunas University of Technology, Studentų 50, LT-51368 Kaunas, Lithuania*
[2]*Institute of Physical Electronics, Kaunas University of Technology, Savanorių 271, LT-50131Kaunas, Lithuania*

Received 05 May 2009; accepted 09 July 2009

The evaporable getters (gas absorbing materials) are widely used in industry in all applications where it is necessary to maintain required vacuum and to assure long lifetime of the operating systems through the sorption of undesired gases. One of the main factors influencing gas sorption characteristics of such getter films is physico-chemical nature of their surfaces. In this research the thin barium getter films have been prepared on glass substrates by thermal evaporation method. Adsorption properties of evaporated barium films formed in the presence of reactive (O_2) and inert (Ar) gas atmospheres by means of *in-situ* and *ex-situ* measurement facilities were analysed. An overall view of the films *in-situ* and *ex-situ* results shows that the best sorption performance of the Ba films was obtained when the Ba film was porous (high vacuum cases) and short-time of evaporation was used. It was found that the sorption properties of particular barium film depend on duration of evaporation process that should be considered together with the residual gas pressure as a parameter influencing porosity of getter film. In conclusion it is evident that the process of barium evaporation must be short-term and forced with respect to temperature, in order to obtain good sorption and structural characteristics of the barium film.

Keywords: thin films, surface properties, barium getters, gas sorption.

1. INTRODUCTION

In the vacuum technique, more in particular in the technique of electronic devices, where enclosed and evacuated spaces (bulbs, tubes and etc.) are used, gas binders are employed, which are commonly named getters. At the end of the pumping process, which is usually carried out by means of pump system (diffusion or mechanical pumps), the pressure in the tubes is not as sufficiently low as it is required for the application. The main purpose of the getter used in such tube is to bind the remaining gases in the envelope and also to get all those gases, which are produced during subsequent operation of the device. The gases in vacuum devices with getter included are removed by chemisorption process. Chemisorption is the binding of gas or vapour on the surface or within the molecular structure of a solid by valence bonds. This usually leads to permanent removal of the gas by the formation of stable, low-vapour-pressure compounds [1, 2].

The active ingredients in evaporable getters are chemically active metals. Mostly the barium is used, which is precipitated as a deposit on the inner side of glass envelope by evaporation from solid getter mixture. Accordingly, these getters are called evaporating or 'flashed' getters. The solid getter mixture commonly is based on a mixture of a $BaAl_4$ alloy and Ni powders, filling a stainless steel ring- or wire shaped container. One of the difficulties in using pure Ba as a getter material is that of retaining its purity before use. Because of its high chemical activity it must be protected during storage from the atmosphere, particularly against oxygen and water vapour. For this reason $BaAl_4$ alloy is used instead of pure Ba, but nonetheless it is recommended to make up the getters just prior to use or else store them in a protective atmosphere or in vacuum [1 – 3].

Flash getters are made in a form that can be easily evaporated and deposited as a thin film on the vacuum envelope or on other cool inactive parts of the structure. Evaporation is produced by induction heating or by the direct passage of electric current through the getter by external leads. Care should be taken in flashing the getter not to overheat it, as evaporation of the Fe (from container) may result in formation of the Ba film, making it ineffective as a getter. The getter should not be placed too close to the area on which the film is to be deposited, as this may produce overheating, resulting in outgassing of the surface and also restricting the film area [4].

The chemical activity of the barium film is extremely high, which makes it capable of absorbing active gas molecules such as CO, CO_2, N_2, O_2, H_2O, H_2 outgassed from the chamber components. The barium film, however, does not absorb rare gases such as argon, helium or krypton. These gases are not chemically active with barium or any other element [1 – 5]. The absorption speed and capacity of the Ba film depends on its extension, its porosity, and its thickness [3]. If the film area is large, the total pumping speed of the Ba film will also be high. The physical characteristics of the Ba film strongly depend on the ambient pressure during the evaporation, on the temperature and cleanness of the surface where the Ba film is formed. The best sorption performances of the Ba films are obtained when the Ba film is very porous. In this respect, low temperature of the surface and relatively high pressure of inert gases allow the formation of very porous Ba films with good sorption performances [3].

The most industrially proven Ba getter application is the cathode ray tubes (CRTs), where large surfaces are available for the deposition of an evaporable barium film. The vacuum tubes with barium getters are still used for

*Corresponding author. Tel.: +370-37-313432; fax: +370-37-314423.
E-mail address: *audrius.giedraitis@stud.ktu.lt* (A. Giedraitis)

very high voltage and high-powered applications. With the modern technology that is available today, the Ba-based evaporable getters also playing very important role in the evacuated heat pipe solar collectors industry. A solar collector absorbs solar radiation and converts it into the heat (photo-thermal conversion). The maintenance of vacuum for the lifetime of the collector (which is typically 20 years) is the key issue for the same getters as used in CRTs. The getter is evaporated in the sealed collector after vacuum processing and a Ba film is created at one of the ends of the collector [6].

The purpose of the experiments reported here was to study adsorption processes and physico-chemical nature of the formed thin barium films, in dependence on the deposition pressure and ambient atmosphere.

2. EXPERIMENTAL DETAILS

2.1. Getter handling and Ba film evaporation

Two types of commercially available barium getter sources were received in an evacuated glass container: ST15A/15KLS/150(WS5) and ST15/20KLS/200(VS 110°), with nominal barium yield of 150 mg and 200 mg, respectively. The form of both particular getter devices is stainless steel ring container filled with a powdered barium-aluminum alloy ($BaAl_4$) mixed with metallic nickel (Ni) powders. Both gettering mixtures are made by SAES getters (Italy) and differ from each other depending on the $BaAl_4$/Ni ratio used. Aforementioned getters after the envelope opening were quickly stored under vacuum until use.

Thin Ba getter films preparation was performed by thermal evaporation method. The principle scheme of a vacuum set-up was the same as in detail reported in the previous experiments [7]. Glass microscope plates from Menzel Glaser (Germany) were chosen as substrates for Ba getter films deposition. The Karl Suss automatic scriber "RA-120" (Germany) equipped with a microscope was used for precise cleaving of the substrates. The plates with a thickness of 1 mm were cut into (13×13) mm^2 pieces, degreasing them by using both boiling in organic solvents (dimethylformamide, with boiling temperature of $T = 153$ °C and acetone, boiling temperature $T = 56.53$ °C) and drying (by clean air or nitrogen) procedures. Next, the getter device (open steel container with powder mixture inside) was quickly weighed and then mounted on the high current feedthrough in the evaporation chamber. Additionally, a few prepared glass substrates were placed on a special holder and mounted over the evaporation source (getter) too. The distance between the evaporation source and substrate was kept constant (120 mm) in the all experiments. After installation of new getter and substrate, the vacuum system was evacuated by means of rotary vane and turbomolecular pumps. The ultimate high pressure in the evaporation chamber was achieved after about 1.5 hour and it was about $8 \cdot 10^{-4}$ Pa. Then the desirable deposition pressure for separate experiment was controlled by inlet in to the chamber one of two gases (Ar or O_2). It means that experiments were carried out in two different atmospheres and the getter films were deposited in the presence of reactive (O_2) or inert (Ar, non-reactive) gases with a purity of 99.999 %.

After the desirable pressure for the particular experiment was achieved, the evaporation process of thin Ba film starts. When the getter container is properly heated to a high enough temperature, the getter releases barium very rapidly, due to the exothermic reaction between aluminium and nickel, which occurs above 800 °C. This reaction increases the getter temperature from 800 °C to 1200 °C in a fraction of a second and initiates barium evaporation. The chemical formula describing this reaction is [2]:

$$BaAl_4 + 4Ni \rightarrow Ba\uparrow + 4NiAl\,. \quad (1)$$

An example of the getter temperature evolution during the heating process is shown in Fig. 1. The time that elapses between heating switch-on and the beginning of the exothermic reaction is called start time. The total time is, therefore, the duration of the external getter heating process.

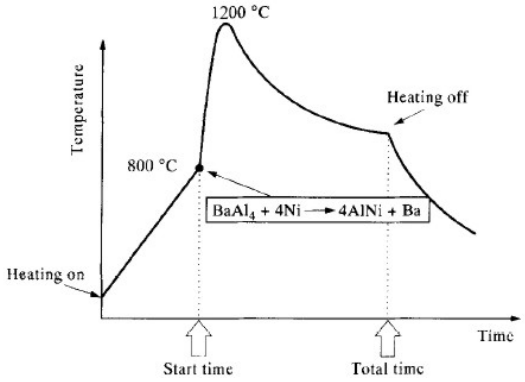

Fig. 1. Temperature evolution during the heating process of barium getter [2]

Once Ba releases in the gas phase at that time the sorption (pumping) process starts, subsequently the Ba atoms condenses on the bare glass substrate surface by producing thin film. The formed film remains an *in-situ* pump.

Under the stated conditions, the time required for the reaction of $BaAl_4$ and Ni to go exothermic as evidence by the sudden increase in getter temperature, mostly was in the range from 19 s to 26 s and from 10 s to 13 s for ST15A and ST15 getters, respectively. The deposition rate then was obtained dividing film thickness (200 nm) by the mentioned deposition time. Typically, the rate was approximately about 10 nm/s and 20 nm/s for ST15A and ST15 getters, respectively.

After the film formation and obtaining the experimental data, the getter device was removed from the vacuum system and immediately weighted to determine the amount of barium evaporated during experiment. Upon exposure to the atmosphere, the weight changes with time as a result of reaction with atmospheric contaminations, such as water vapour and oxygen. The amount of barium evaporated under the stated conditions is in the range from 70 mg to 90 mg. This yield results in barium film thickness (200 nm) comparable to that obtained in commercially produced CRT tubes [8,9].

2.2. Characterization of getter mixture

XRD measurements were done in order to characterize the crystalline structure of as received (before evaporation)

getter mixtures. The DRON 3.0 diffractometer (Bourevestnik Inc., Russia) with standard Bragg.-Brentan (θ:2θ) focusing geometry using CuKα radiation (wavelength 0.154178 nm) was used. The crystallite size of getter grains was estimated from the Scherrer's equation [10].

The morphology of getter mixtures has been examined by environmental scanning electron microscope (ESEM) Quanta 200 FEG (FEI Ltd, Eindhoven, Netherlands), coupled with an energy-dispersive X-ray microanalysis (EDX) spectrometer Quantax 200 (Bruker, Germany) equipped with Xflash 4030 detector. ESEM micrographs of powdered surfaces were obtained in high pressure regime, at an accelerating voltage of 5 kV by Everhart Thornley secondary electron detector (ETD). EDX studies were carried out in high pressure regime by ETD detector, at an accelerating voltage of 20 kV, at working distance of 10 mm and magnification of 1000×, with the distribution mapping elements from the surface of getter mixture. The weight percent concentrations of individual surface precipitates have been calculated automatically by EDX software.

2.3. Experimental set-up for in-situ growth control of thin Ba getter films

The three different physical parameters (thickness of growing film, temperature of getter source and optical transmittance of growing film) were measured *in-situ* during thin barium film deposition process. The deposited barium film thickness was evaluated by a quartz microbalance thickness monitor QM-331 (Veeco, Germany) placed in close proximity to the substrate. The calibration of the quartz microbalance was obtained by independent thickness measurements carried out by using an NT-206 atomic force microscope with Surface View software (Microtestmachines Co., Belarus). *In-situ* temperature measurement was performed by thermocouple placed near the source-ring container bottom outer edge. The thermocouple of type N was used, because it is suitable for use at high temperatures, exceeding more than 1200 °C.

Evaluation of the optical transmittance of film/substrate system in real time scale was performed by using the simple transmittance sensor. Both devices (thermocouple and transmittance sensor) were equipped with the wireless RF data transfer allowing real time control of temperature ant transmittance parameters by the program based on Visual Basic software package. More details about calibration of optical transmittance sensor and suitability to control kinetics of growth of the films (Ag, Ba getters) and adsorption phenomena from the residual gases one can find in the previous study [7].

2.4. Thin Ba films ex-situ experimental equipment

The obtained thin Ba films were removed from evaporation chamber for further *ex-situ* examination. A range of physico-chemical techniques employed for characterization of films included environmental ESEM, atomic force microscopy (AFM), X-ray photoelectron spectroscopy (XPS) and optical spectrometry.

For observing the microscopic nature of the thin films the same ESEM Quanta 200 FEG (like for getter mixture analysis) was used. Micrographs of the film surfaces were obtained in low pressure regime with the large field detector (LFD) suited for secondary electron registration. Quantitative measurements of porous film microstructure (such as porosity and shape) were carried out by image analysis. The software in the form of a plug-in [11] for a free software "ImageJ" [12] was used.

Surface morphology of thin films was examined by AFM in contact mode using NT-206 multifunctional scanning atomic force microscope with Surface View software (Microtestmachines Co., Belarus). Two-dimensional and three-dimensional images of the surface and determination of its roughness were analysed.

XPS technique was employed to study the composition of the films, atomic surface concentrations and formed chemical bonds. XPS spectra were recorded using XSAM 800 (KRATOS Analytical, UK) spectrometer. X-ray source with Al Kα ($h\nu$ = 1486.6 eV) anode, a 90-degree takeoff angle was used. The samples were analyzed as received – no surface cleaning (by Ar^+ ion source) procedure was applied. The carbon, oxygen and barium relative atomic concentrations were calculated from the appropriate peak area with respect to the sensitivity factors, using original KRATOS Analytical software DS800. Charge effects were compensated assuming carbon C1s peak at 284.75 eV position.

The *ex-situ* optical absorption measurements of Ba thin films were performed at normal incidence by UV/VIS and NIR spectrophotometer AvaSpec 2048 (AVANTES, Netherlands) in the region of wavelengths 200 nm – 1100 nm. The optical reflectance and transmittance spectra were recorded by using Avasoft software.

3. EXPERIMENTAL RESULTS

3.1. Characterization of evaporable getter mixture

First of all, characterization of evaporable materials was carried out. When combined with techniques such as XRD and ESEM coupled with EDX spectrometer, detailed information regarding evaporable material (powder) components, their size, quantitative composition and structure can be obtained. XRD patterns of two getter powder types (ST15A and ST15) are shown in Fig. 2.

Since X-ray diffraction peaks are known to become broader as the particle size decreases, analyzing diffraction peaks of both samples according to the Scherrer's formula it was estimated that the crystallite size was less than 20 nm. The calculated size of Ni crystallites was approximately 17 nm. Also it was found that there is some discrepancy in crystallite size estimation for different Al_4Ba peaks (or for diffraction on different planes) as shown in the Table 1. This may be explained by a high anisotropy of a particle structure containing a lot of defects.

To further elucidate the size and crystal structure of aforementioned materials, ESEM secondary electron image for both samples was taken at magnification of 1000×, as shown in Fig. 3 (a, d). Surface morphologies show the presence of flake-like particles of irregular shape with typical size from hundreds of nanometers to a few tenth of microns, many of which appear covered by numerous smaller rounded agglomerate-like structures. In

Table 1. Calculated particle sizes *d* (nm) from XRD data of Al_4Ba crystals for two analysed samples

Getter type: ST15A			Getter type: ST15		
Crystal planes	FWHM*	d ,nm	Crystal planes	FWHM*	d ,nm
(110)	2.025	4.0	(110)	2.001	4.1
(103)	0.596	13.8	(103)	0.664	12.4
(112)	0.554	14.9	(112)	0.581	14.2
(200)	0.499	16.9	(200)	0.893	9.5

*FWHM – peak full-width at half-maximum.

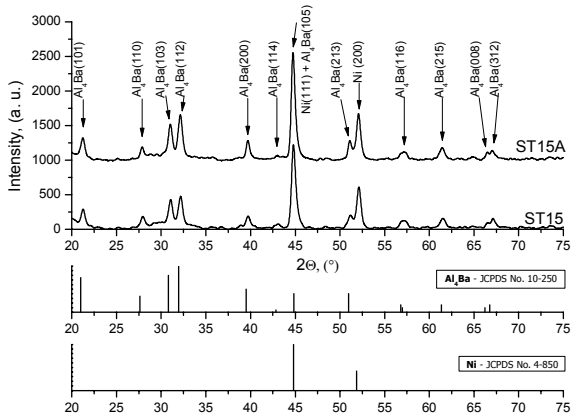

Fig. 2. XRD patterns of ST15A and ST15 barium getter crystals (underneath the JCPDS data for two different phases obtained are shown)

respect of particle shape, observed Al_4Ba phase particles are appreciably bigger than the Ni phase particles. The size of the nanocrystallites determined by the Scherer equation from XRD measurements is smaller than the particle size values measured from ESEM micrographs, shown in Fig. 3. This can be explained by the existence of different crystalline domains in the particles. Thus the particle size measured in ESEM corresponds to the polycrystalline grains and it is bigger than the crystallite size given by XRD.

Elemental maps recorded using ESEM-EDX analysis by registering secondary electron images were used to confirm the composition of each particle. The presented nearly identical X-ray energy spectra for preserved areas from ESEM microphotography (of Fig. 3, a, d) demonstrates the distribution of three main components Al (K shell X-ray), Ni (K shell X-ray) and Ba (L shell X-ray) from which the barium getter has been manufactured (Fig. 3, b, e). From the EDX spectrum one can point out the presence of iron (Fe) on the surfaces of samples, because the examination of samples was carried out directly from the stainless steel container, filled with particular getter powders mixture. Since the thickness of the getter mixture is of the same order as the depth analysis by EDX, for that reason the Fe peaks corresponding to the getter container were registered. Both other remained components are common atmosphere contaminations (C, O). The visual elemental distribution of the three main elements identified, for the surfaces of the both ESEM preserved areas, are shown in (Fig. 3, b, e).

Table 2 presents the quantitative composition of analysed getters determined by EDX, measured at the surfaces of examined samples, in the preserved areas from ESEM microphotography. Comparing our obtained and manufacturer reported technical data (Table 2, bottom) on barium getter weight percent concentrations (for the main mixture constituents) it was found that particular quantities were close to coincidence.

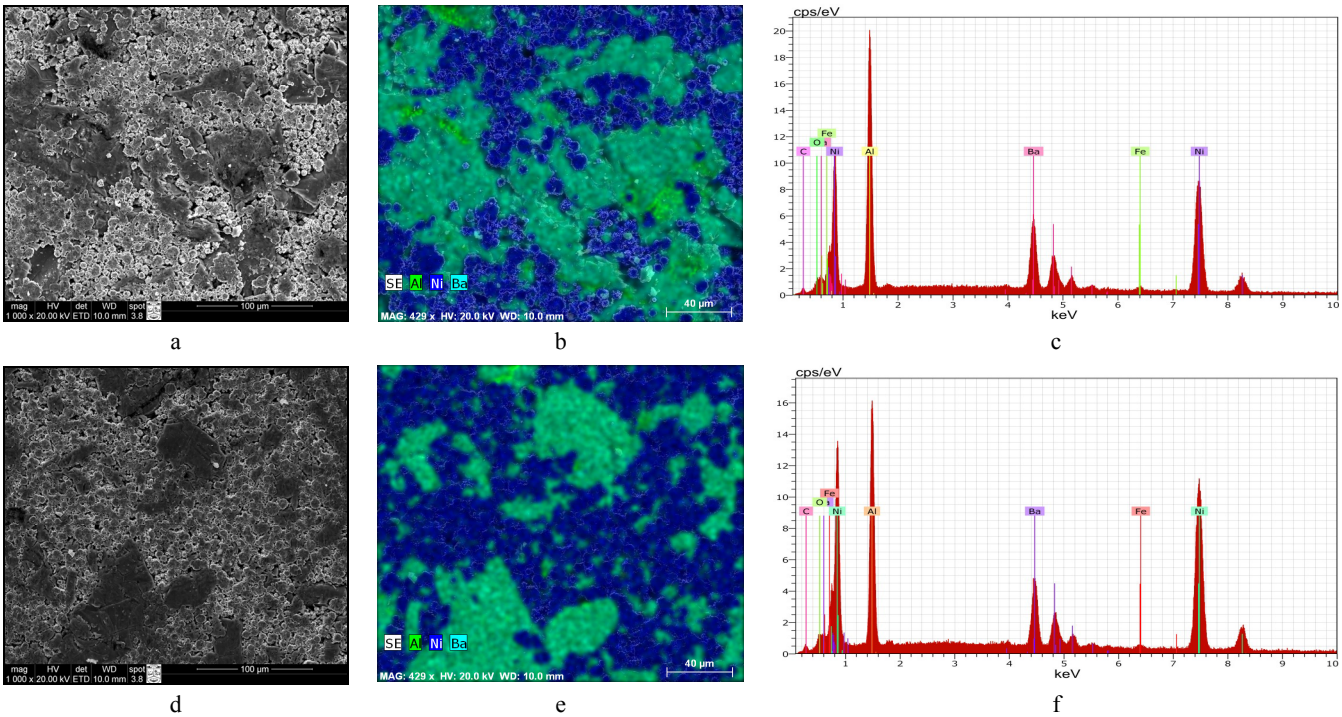

Fig. 3. (in colour on-line) ESEM-EDX data for ST15A (a, b, c) and ST15 (d, e, f) types of barium getters. From top to bottom: ESEM secondary electron microphotographs (a, d); EDX mapping images of Al (K shell X-ray), Ni (K shell X-ray) and Ba (L shell X-ray) (b, e) and X-ray energy spectrum for entire area of ESEM image (c, f)

Table 2. Quantitative composition of getter sample surfaces

Element	Series	Getter type			
		ST15A		ST15	
		Weight percent [%]	Error[[%]	Weight percent [%]	Error [%]
Al	K-series	30.65	1.4	24.39	1.1
Ni	K-series	43.57	1.1	53.69	1.4
Ba	L-series	22.59	0.6	18.71	0.5
C	K-series	0.99	0.2	1.09	0.2
O	K-series	0.79	0.2	0.96	0.2
Fe	K-series	1.41	0.1	1.14	0.1
Total:		100		100	
Manufacturer data for three main components [13, 14]:					
Nominal composition (wt%)		21 % Al 55 % Ni 24 % Ba		22 % Al 53 % Ni 25 % Ba	

3.2. In-situ growth control of thin Ba getter films

The two types of aforementioned getter materials ST15A and ST15 were used as sources for the thin barium films (as gas adsorbents) deposition on glass substrates. Two sets of barium getter films with the same thickness (200 nm) were deposited in two different gas atmospheres (Ar, O_2) by the thermal evaporation method. The evaluation of adsorption processes during thin film growth was done in dependence on the deposition pressure and film formation atmosphere. The developed optical sensor was applied to follow absorbance of the growing film (at wavelength $\lambda = 565$ nm) and kinetics of the gas adsorption from the ambient during (or after) Ba getter film deposition. Optical absorbance (neglecting film reflectance) was registered *in-situ* measuring optical transmittance of the film-substrate structure. Examples of the optical absorbance dependence on time scale for the ST15A type barium films, formed in two different atmospheres, are shown in the Fig. 4. The typical time dependent experimental process consists of several parts:

First point. First point of optical absorbance curves ($t_s = 0$ s) corresponds to the time moment when exothermic reaction described by (1) equation begins. In other words, this is a time when the getter material placed in the vacuum chamber was heated to a high enough temperature, in order to initiate barium evaporation. For that reason it is called start time (t_s).

Dot vertical line (t_g) is attributed to the time that elapses between initiation and beginning of the exothermic reaction or film growing process. For that reason it is called film growing time (t_g). At this moment of time the getter heating is switched-off. The nearly maximum absorption (or minimum transmittance) reached at this time moment shows that barium mirror was formed nearly in all film growing regimes, except the particular low vacuum cases (at $p = 7.0 \cdot 10^{-1}$ Pa for Ar atmosphere (Fig. 4, a) and $p = 1.2 \cdot 10^{-1}$ Pa for O_2 atmosphere (Fig. 4, b)). Because of small mean free path of evaporable particles and their multiplex collisions with gases or vapour particles [4] the aforementioned pressures are attributed to extreme low vacuum cases, at which the deposition of films it was hardly possible.

Dashed vertical line (*TM off*). It corresponds to the pumping system turbomolecular (TM) pump switching-off. The time marked as t_1 it's equal to 3 min., showing the time interval after the film was formed. No evidence on formed barium films adsorption variation was found in this time scale (except low vacuum cases), because high enough vacuum was secured by means of TM. The other part of optical absorbance dependence on time was attributed to the system outgassing process time interval, when the valve of TM pump was closed. The (t_2) duration selected was about 1 min. As one can see, no optical changes conditioned by outgassed gases were obtained per such short time interval.

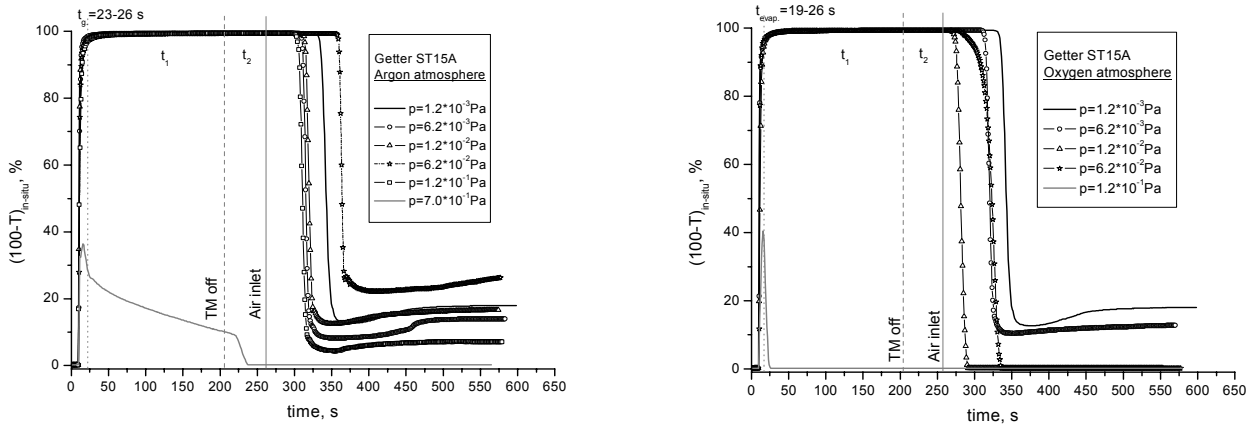

a b

Fig. 4. Optical absorbance of the ST15A barium getter-glass system during and after evaporation of getter material and adsorption of residual gases: a – for the films evaporated in inert Ar atmosphere; b – for the films formed in presence of reactive O_2 atmosphere

Solid vertical line (*Air inlet*). This experimental stage indicates the simulated film adsorption experiments in static conditions, without any external pumping. The maintained pressure in the chamber after barium film formation was destructed by inlet the air in the chamber. In this time regime (Fig. 4) the variation of *in-situ* optical absorption is dependent only on getter film sorption phenomena. The time dependent optical absorption studies in both formation atmospheres shows that after film exposure to the air the more or less transparent films, with the transmission values higher than 70 %, were observed.

The obtained optical transmittance increase (or absorbance decrease) can be explained by interaction of chemically active film and residual gas. It is known [15], that once the barium getter has been released, the barium/gas reactions takes place and sorption (pumping) process starts, while the total pressure of residual gases in the vacuum envelope decreases.

The barium film also provides a clear visual indicator as an evidence of the vacuum status and reaction occurred. The silver colored barium film turns a white color if the vacuum is ever lost and indicates that reaction between barium film and atmospheric oxygen occurred. The films taken from the chamber at the end of our *in-situ* experiment confirmed that white colored films were formed.

Simultaneous measurements of the typical getter temperature evolution for the same ST15A getter films are shown in Fig. 5.

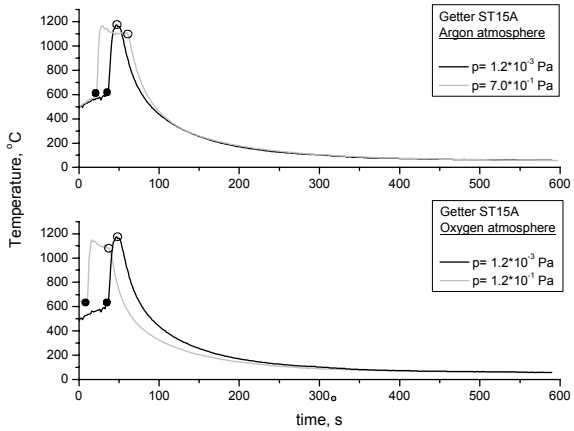

Fig. 5. Typical temperature evolution of simultaneously measured ST15A getter films for both extreme low and high vacuum cases (filled and unfilled circles corresponding to initial and ultimate films growth stages)

Temperature curves clearly reveal exothermic reaction character [2], by means of explosive change in the temperature form more than 600 °C to about 1200 °C during the heating (film growth) process. The filled and non-filled circles on temperature curves correspond to the initial (t_s) and ultimate (t_g) time moments of film growth, respectively (Fig. 5). The duration of film growth process then can be estimated by difference between these two points in accordance with pressure. The analysis of time dependent temperature curves shows that the duration required for the proper thickness film deposition in extreme low vacuum cases were few times higher by comparing them with those obtained in high vacuum.

3.3. Ex-situ characterisation of thin Ba getter films

The aforementioned critical cases of the films (ST15A type) formed in the high vacuum ($p_{Ar,O2} = 1.2 \cdot 10^{-3}$ Pa) and poor vacuum ($p_{Ar,O2} \geq 1.2 \cdot 10^{-1}$ Pa), under our experimental conditions, were selected for the further in-deep analysis. The selected samples were marked regarding to the film formation atmosphere and deposition pressure as shown in the Table 3.

Table 3. The list of samples used for in-deep examination

Getter type	Sample code	Gas atmosphere	Deposition pressure, Pa	Vacuum status
ST15A/ 15KLS/ 150(WS5)	#1(Ar)	Ar	$1.2 \cdot 10^{-3}$	high
	#2(Ar)		$7.0 \cdot 10^{-1}$	poor
	#3(O_2)	O_2	$1.2 \cdot 10^{-3}$	high
	#4(O_2)		$1.2 \cdot 10^{-1}$	poor

The four micrographs of barium film surfaces, each 7.46 μm × 6.87 μm in size, were recorded at the same magnification by using ESEM and are given in Fig. 6. According to these data, the barium film surfaces displayed ridged nanostructure consisting of spherically shaped nanoparticles with different 20 nm – 30 nm sizes, not uniformly distributed on the surface. One can also see that nanoparticles were coupled in to the groups and elongated clusters (about 500 nm – 1000 nm long) were formed.

In general, it is necessary to prevent sintering and to obtain a porous layer of accumulated barium particles [2]. A porous layer exposes a large surface for the gas atmosphere, thus promoting good gettering performance. This porous layer also increases the number of collisions of gas molecules with the barium film. Quantitative measurements of porous film microstructure (such as porosity and shape) were carried out from SEM imagery by image analysis. The results of quantitative pores analysis are presented in Table 4. The main parameter porosity was defined as the percentage of pore area with respect to the total sampled area. Furthermore, a set of numerical descriptors was used to characterize particles on each of shown ESEM micrographs (Fig. 6) and analysis was performed to produce four shape and size parameters contained in ASTM F1877-98 for each particle [16]. These descriptors are equivalent circle diameter (ECD), aspect ratio (AR), roundness (R), and form factor (FF). ECD is a measure of size defined as the diameter of a circle with area equivalent to the area of the particle, and has units of length. AR is defined as the ratio of the major diameter to the minor diameter. The major diameter is the longest straight line drawn between any two points on the outline. The minor diameter is the longest line perpendicular to the major diameter. R is the measure of how closely a particle resembles a circle, and varies in magnitude from 0 – 1, with a perfect circle having a magnitude of 1. FF is similar to roundness, but is based on the perimeter of the particle outline rather than the diameter. With reference to pore shape descriptors used the particles can be categorized into rounded, elongated and irregular based on the following criteria. Rounded particles were those with $R > 0.7$, and elongated particles those with $AR > 2.7$. Particles that remained are categorized as irregular [16].

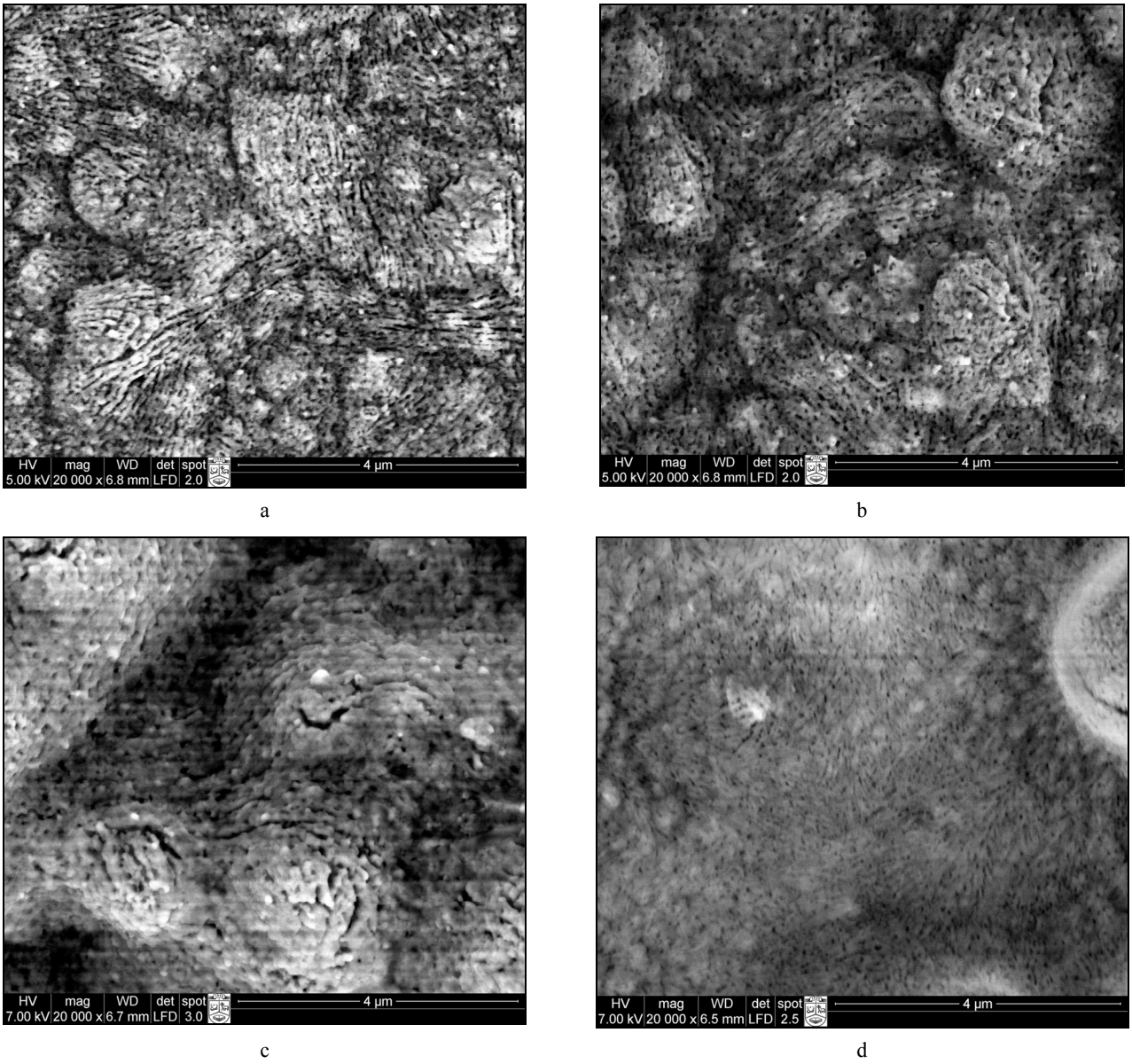

Fig. 6. ESEM-SE images of the barium films grown in two different atmospheres and pressure ranges: a – $p = 1.2 \cdot 10^{-3}$ Pa (Ar atmosphere), b – $p = 7.0 \cdot 10^{-1}$ Pa (Ar), c – $p = 1.2 \cdot 10^{-3}$ Pa (O_2), d – $p = 1.2 \cdot 10^{-1}$ Pa (O_2). With a magnification of 20000× and scale – 4 µm

Table 4. Quantitative results of porous films microstructure

Sample code	#1(Ar) [Fig. 6 (a)]	#2(Ar) [Fig. 6 (b)]	#3(O_2) [Fig. 6 (c)]	#4(O_2) [Fig. 6 (d)]
Pores detected (counts)	2558	2662	1450	1886
Porosity (%)	23	18	14	6
<ECD> (nm)	57.77 ±43.65	49.84 ±37.33	56.43 ±46.25	36.53 ±20.98
<AR>	1.77 ±0.69	1.64 ±0.54	1.69 ±0.59	1.68 ±0.55
<R>	0.44 ±0.16	0.47 ±0.14	0.46 ±0.15	0.49 ±0.13
<FF>	0.42 ±0.16	0.45 ±0.14	0.44 ±0.14	0.50 ±0.11

Results expressed as value ± standard error. <ECD> – mean equivalent circle diameter; <AR> – mean pores aspect ratio; <R> – mean pores roundness; <FF> – mean pores form factor.

Examination of the surfaces by imaging technique showed that the films grown in the inert Ar gas atmosphere exhibit a more porous structure (#1(Ar), #2(Ar) samples) than that of the film grown in the presence of O_2 atmosphere (#3(O_2), #4(O_2) samples) as shown in the Table 4. The increase of the deposition pressure in the deposition chamber drops films porosity by 22 % and 57 % in consideration of Ar and O_2 atmospheres, respectively. As one can see, large openings called macropores (diameter greater than about 50 nm) are dominant in the

samples #1(Ar) and #3(O_2) (formed in a high vacuum).The smaller pores called mesopores (diameter from about 2 nm to 50 nm) are present in the films formed in the poor vacuum (samples #2(Ar) and #4(O_2)).

An AFM has been used to obtain three-dimensional characterization of the surfaces of aforementioned structures and determination of their roughness. The obtained images for all four samples are shown in Fig. 7. The AFM measurements (Fig. 7) confirm depth and shape variation of the barium films registered with the ESEM. The ESEM and AFM results indicate that the barium films have non-uniform character with the elongated agglomerates, of about 500 nm – 1000 nm long, randomly distributed on barium surface. The rms roughness R_q of films formed in Ar atmosphere (#1(Ar), #2(Ar) samples) varied between 200 nm to 51 nm and for the films formed in O_2 atmosphere – from 200 nm to 300 nm (#3(O_2), #4(O_2) samples, respectively). Sample #2(Ar) (in the poor vacuum) shows a smooth surface texture with a low rms roughness of the order of 51 nm, which considerably reduces pores and voids on the surface (Fig. 7, b). The suchlike results were expected for the sample #4(O_2) (in O_2 atmosphere, Fig. 7, d), but due to open craters and cracked structures formed the rms roughness even bigger than for films formed in high vacuum (Fig. 7, a & c) was observed.

Optical constants for the same four vacuum evaporated thin films were calculated from reflectance and transmittance spectra. Fig. 8 shows the dependence of the optical transmission (T) and reflection (R), respectively, of the investigated thin film samples with the wavelength (λ). It is seen from the graph of Fig. 8, a) that the values of the transmittance is low for the films grown in the high vacuum (#1(Ar), #3(O_2)) in respect of the films formed in the poor vacuum (#2(Ar), #4(O_2)). It is also observed from the graph of Fig. 8, a and b) that the values of transmittance and reflectance are low in the ultraviolet region for all samples. In the visible region it is seen the increase of the transmittance and reflectance whereas reflection decreases in the near-infrared region.

The optical absorption coefficient (α) of the films was evaluated from the optical transmittance (T) and reflectance (R) data using the relation:

$$\alpha = 1/d \ln [T/(100 - R)^2], \quad (2)$$

where d is the thickness of the film. The band gap (E_g) is related to the absorption coefficient (α) by the relation:

$$\alpha h\nu = B(h\nu - E_g)^{\eta}, \quad (3)$$

where $h\nu$ is the photon energy, B is a constant, and η is a constant that depends on the types of transitions involved. η = 1/2, 3/2, 2, and 3 for direct allowed, direct forbidden, indirect allowed, and indirect forbidden transitions, respectively [17].

We assumed the direct transition between the top of the valence band and the bottom of the conduction band in these films, which fitted to the relation $\alpha h\nu = B(h\nu - E_g)^{1/2}$. The optical band gap ($E_g$) of the investigated films was estimated from the intercept of the plot of $(\alpha h\nu)^2$ versus photon energy ($h\nu$). The optical band gap of the films was

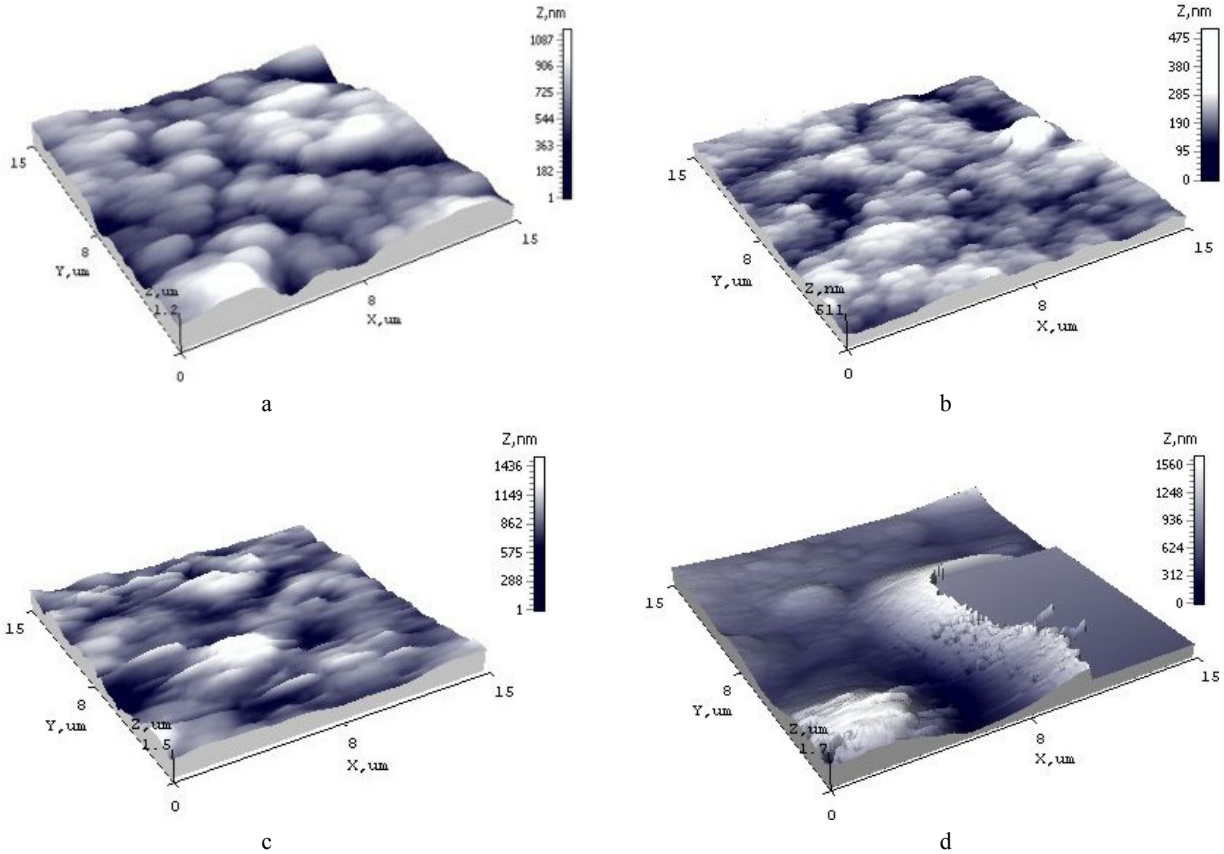

Fig. 7. AFM results indicating the 3D images for thin barium films in dependence of pressure and atmosphere: a – $p = 1.2 \cdot 10^{-3}$ Pa (Ar atmosphere), b – $p = 7.0 \cdot 10^{-1}$ Pa (Ar), c – $p = 1.2 \cdot 10^{-3}$ Pa (O_2), d – $p = 1.2 \cdot 10^{-1}$ Pa (O_2). Film surfaces were examined in contact mode, the size of the images 15.4 μm × 15.4 μm

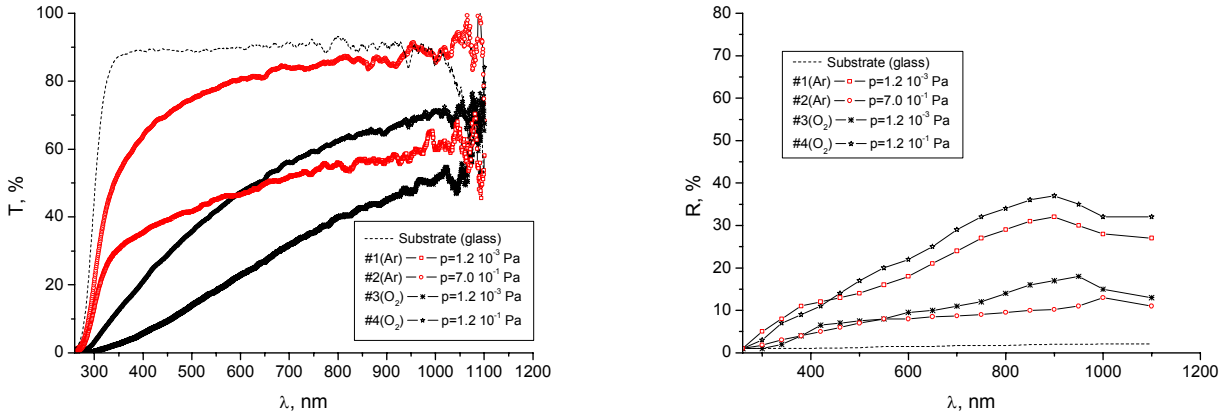

a b

Fig. 8. The variation of transmittance (a) and reflectance (b) with the wavelength in the range from 260 nm to 1100 nm. Samples marked regarding to the data of Table 3

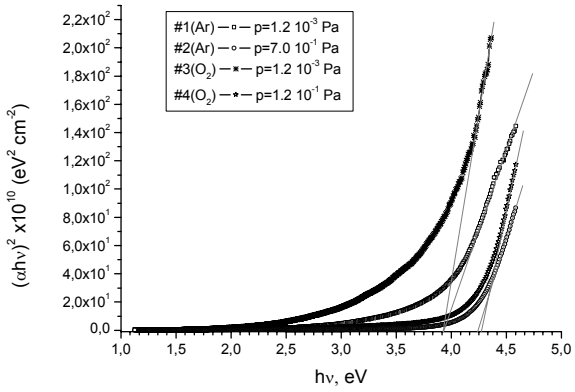

Fig. 9. The plots of $(\alpha h\nu)^2$ versus photon energy for the investigated films

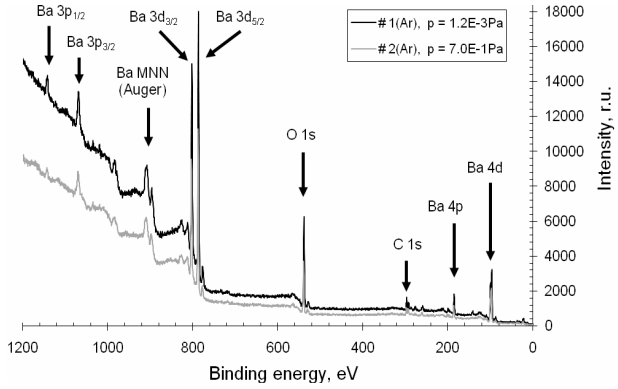

Fig. 10. Typical XPS survey spectra taken for thin barium films formed in the presence of Ar gas. Deposition pressures are shown in legend

determined to an accuracy of ±0.01 eV. Fig. 9 shows the plots of $(\alpha h\nu)^2$ versus photon energy of deposited films at different pressure ranges. The extrapolation of the linear portion of the plots to $\alpha = 0$ resulted the optical band gap of the films. The values of the direct energy gap for the films formed in the high vacuum was (3.90 ±0.01) eV (#1(Ar), #3(O_2) cases) and for the films formed in poor vacuum – (4.30 ±0.01) eV in Ar atmosphere (#2(Ar)) and (4.35 ±0.01) eV in O_2 atmosphere (#4(O_2)).

It is suggested that the direct energy gap may represent the onset of intrinsic absorption of the film while the indirect energy gap may represent the onset of absorption involving some defect states [17]. No values for the direct energy gap of barium films has been reported, therefore is not possible to compare our obtained energy gap values.

The surface composition of the barium films, their concentrations and formed chemical bonds were investigated by XPS technique. The typical XPS survey spectra of barium films (#1(Ar) and #2(Ar)) deposited in Ar atmosphere are presented in Fig. 10. Both spectra present Ba 3p, Ba 3d, Ba 4p, Ba 4d, O 1s and C 1s core-levels, as well as the corresponding Ba MNN Auger decay in the high energy range of 890 eV – 910 eV. It means that three types of basic element atoms (barium, oxygen and carbon) exist on the surface of the barium films. It is evident, that except main barium element, the oxygen (indicated by the O 1s peak at 538.88 eV) and carbon (indicated by the C 1s peak at 284.75 eV) are the common contaminants of atmosphere detected on surface [18, 19]. These oxygen and carbon atoms are due to contamination in the deposition chamber and environmental pollution during handling and storage.

Equally, we might say that for all four barium films the XPS peaks of aluminium and nickel were not observed, considering that starting materials used in evaporation process were powders of $BaAl_4$ alloy and Ni. The Si peaks characteristic for substrate (glass) there was not found too. Last-mentioned fact not-directly corresponds that homogeneous films were formed.

The calculated surface atomic concentrations for all examined samples are listed in Table 5. As one can see, the calculated oxygen amount is noticeably bigger than that which is probable for stoichiometric barium oxide (BaO). It shows that the big amount of absorbed oxygen exists on the surface of samples. And conversely, the amount of atmospheric carbon contaminations matches known values

[18, 19] in the case when no surface bombardment was done before surface investigation.

Table 5. Surface atomic concentrations calculated for Ba films

Element	Sample code			
	#1(Ar)	#2(Ar)	#3(O_2)	#4(O_2)
Ba 3d	18.1 %	18.0 %	19.3 %	17.0 %
O 1s	62.5 %	61.1 %	65.9 %	62.7 %
C 1s	19.4 %	20.9 %	14.9 %	20.3 %

Fig. 11 shows the high resolution Ba 3d core level spectra for the same two films formed in Ar atmosphere mentioned above. The Ba 3d spectra exhibit spin-orbit components, namely Ba $3d_{5/2}$ and Ba $3d_{3/2}$, at binding energies of about 780.6 eV and 795.9 eV for the both samples, in agreement with literature data [18,19]. One can see, that the difference between Ba 3d peak doublets character and position in the scale of binding energies (BE) is negligible, consequently reliable that barium atoms present the same compounds in all samples. The positions of obtained peaks correspond to few possible chemical states: Ba, BaO and $BaCO_3$ as shown in the Table 6.

Unfortunately, due to small energy difference there is no possibility to discriminate the position of such peaks in the scale of BE.

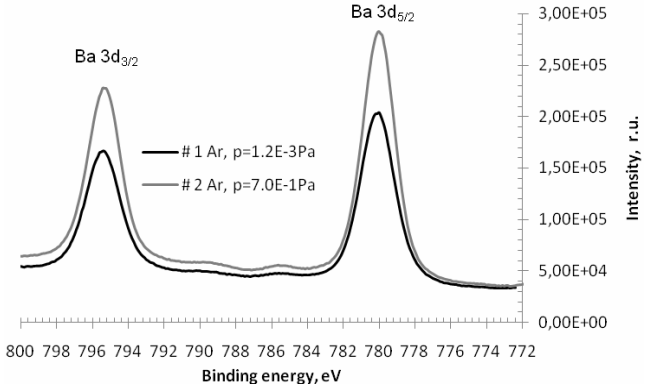

Fig. 11. Detailed binding energy spectra of Ba 3d core level electrons. Deposition pressures are shown in legend

Table 6. The photoelectron binding energies (BE) for Ba 3d doublets in this work and literature [18, 19]

Sample	Obtained BE of core levels, eV	
	Ba $3d_{5/2}$	Ba $3d_{3/2}$
A	780.06	795.39
B	780.01	795.34
C	780.04	795.36
D	780.04	795.37
Chemical states	Known core levels, eV	
	Ba $3d_{5/2}$	Ba $3d_{3/2}$
Ba	780.11	795.31
BaO	779.57	794.92
$BaCO_3$	779.85	–

The typical detailed binding energy spectrum for the sample #1(Ar) is shown in Fig. 12. The width of obtained oxygen peaks typical for all samples and the value FWHM = ~2 eV. In order to estimate relative amounts of possible chemical bonds the broad O 1s peak has been deconvoluted into the four peaks which are marked as peaks A, B, C and D (Fig. 12).

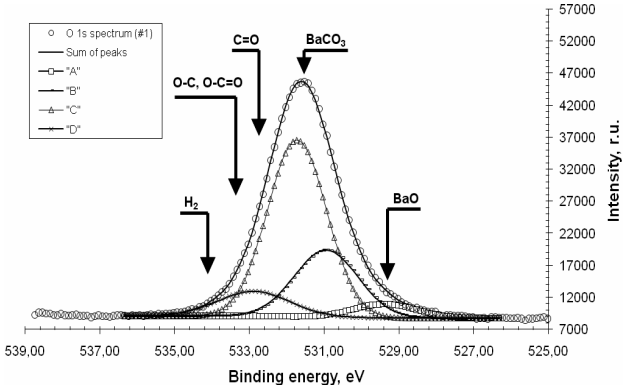

Fig. 12. Detailed binding energy spectra for O1s core level electrons (deconvolution of O 1s bands). The spectrum was deconvoluted into the components, corresponding to the oxidation states of the film marked by the arrows

The arrows in the spectrum show possible chemical states. Chemical bonds relative amounts calculation results and peak positions of known chemical states are shown in Table 7.

Table 7. Obtained relative bonds amounts and known BE of chemical states for characteristic peak O1s position

Sample	Deconvolution of O 1s bands	O 1s BE, eV	Relative intensity, %
#1(Ar)	"A"	529.6	7.80
	"B"	531.1	31.62
	"C"	531.7	54.77
	"D"	533.2	5.81
#2(Ar)	"A"	529.7	7.63
	"B"	531.2	27.13
	"C"	531.6	59.13
	"D"	533.0	6.11
#3(O_2)	"A"	529.5	7.35
	"B"	531.1	30.59
	"C"	531.7	52.82
	"D"	532.8	9.24
#4(O_2)	"A"	529.4	5.08
	"B"	530.9	24.74
	"C"	531.7	59.98
	"D"	532.9	10.20

Chemical states	Known core levels, eV [18,19]
BaO	529.30
$BaCO_3$	531.53
C=O, O–C=O	532.70
C–O	533.30
H_2O	534.01

From Fig. 12 and Table 7 we can conclude that just a little part of barium oxide (BaO) was found on the samples surfaces. The predominant are atmospheric contaminations and their compounds with barium atoms($BaCO_3$). The last fact explains decent-sized oxygen atomic concentrations mentioned in Table 5.

In general, a number of reactions between a barium film and a residual gas are possible in the vacuum envelopes, leading to different reaction products. According to Perdjik [20] the reactions leading to stable compounds formation may be subdivided into three categories: primary, secondary and tertiary reactions, main of them are shown in Table 8. The primary reactions deal with the reactions between a metallic barium film and gases. Besides these primary reactions, other reactions can take place, making more complex the residual gas scenario in the vacuum system. The compounds formed by primary reactions (BaO, BaH_2, BaC_2, Ba_3N_2) may react (secondary reactions) with the gases in the vacuum system as well, and form $Ba(OH)_2$ and $BaCO_3$ compounds. Reactions of the latter compounds with residual gases are called tertiary reactions [20, 21].

The air, which is introduced into the vacuum chamber, under our experiment conditions, consist of nitrogen, 78 %, oxygen 21 % and others 1 %. With respect to that the chemical formulas describing possible barium film reactions with nitrogen and oxygen are:

$$3Ba + N_2 \leftrightarrow Ba_3N_2 \; ; \quad (4)$$

$$2Ba + O_2 \leftrightarrow 2BaO \; . \quad (5)$$

Once the barium has been released during evaporation process the reaction with molecular nitrogen starts resulting in the reaction product of barium nitride (Eq. 4). However, this chemical reaction happens just beside temperature higher than 260 °C [20]. Unbounded molecular nitrogen at the room temperature exhibit chemically inert-like properties and can be absorbed just thanks to physical sorption behaviour of evaporated barium film. Supposedly the main reaction occurs between barium film and oxygen (eq. 5).

Table 8. Examples of primary, secondary and tertiary reactions of residual gases with a barium getter [20, 21]

Primary reactions
$2Ba+O_2 \leftrightarrow 2BaO$ $3Ba+2CO \leftrightarrow 2BaO+BaC_2$ $3Ba+N_2 \leftrightarrow Ba_3N_2$ $Ba+H_2 \leftrightarrow BaH_2$ $Ba+H_2O \leftrightarrow BaO+H_2$ $5Ba+2CO_2 \leftrightarrow 4BaO+BaC_2$ et cetera.
Secondary reactions
$BaO+CO_2 \leftrightarrow BaCO_3$ $BaO+H_2O \leftrightarrow Ba(OH)_2$ $BaC_2+H_2O \leftrightarrow BaO+C_2H_2$ $2BaH_2+O_2 \leftrightarrow 2BaO+2H_2$ et cetera.
Tertiary reactions
$Ba(OH)_2+CO_2 \leftrightarrow BaCO_3+H_2O$ et cetera.

4. CONCLUSIONS

An overall view of the films *in-situ* and *ex-situ* results shows that the best sorption performance of the Ba films, under our experimental conditions, was obtained when short-time of evaporation was used and formed Ba films were porous (high vacuum cases). In this respect, room temperature of the substrate and relatively high pressure of inert or reactive gases didn't allow the formation of very porous Ba films with good sorption performances as was expected [3]. It was found that the sorption properties of particular barium film depend on duration of evaporation process that should be considered together with the residual gas pressure as a parameter influencing porosity of getter film. The extended heating process of getter material (low vacuum cases) gives undesirable influence on the structure of the film, due to few reasons. First of all, in the end of the evaporation process the intensity of barium vapours, due to decreasing of its concentration in the getter material, raises the formation of far smaller particles of barium, which stick to the initially deposited rough barium film surface. For that reason, the grains of the film are trend to amalgamate. Secondly, the extended heating of getter container raises temperature of the close placed substrate therefore the grains of the film are trend to amalgamate too. In conclusion it is evident that the process of barium evaporation must be short-term and forced with respect to temperature, in order to obtain good sorption and structural characteristics of barium film. However, immoderate rush of the evaporation process gives rise to the evaporation of container material, resulting in formation of container metal film over the active barium film.

Acknowledgments

We are grateful to the scientists at Institute of Physical Electronics (KTU), especially to senior researcher Dr. Kęstutis Šlapikas for its support in this and other studies we have carried out. Also to Dipl. engineer Algimantas Juraitis and senior researcher Dr. Asta Guobienė for their precise XRD and AFM measurements, respectively. Special thanks to Dr. Igoris Prosyčevas for his advice and recommendations on this paper.

We also thank Tomas Tamulevičius (Electron Microscopy Facility, Faculty of Design and Technologies, KTU) for carrying out the ESEM-EDX analyses, images and elemental maps on our samples.

REFERENCES

1. **Giorgi, T. A.** Getters and Gettering *Japanese Journal of Applied Physics* 2 – 1 1974: pp. 53 – 60.
2. **Ferrario, B.** Chemical Pumping in Vacuum Technology *Vacuum* 47 (4) 1996: pp. 363 – 370.
3. **Tominetti, S., Amiotti, M.** Getters for Flat-panel Displays *Proceedings of the Institute of Electrical and Electronics Engineers (IEEE)* 90 (4) 2002: pp. 540 – 558.
4. **Lafferty, J. M.** Foundations of Vacuum Science and Technology. John Wiley and Sons, Inc., 1998: p. 403.
5. **Porta, P. della.** Gas Problem and Gettering in Sealed-off Vacuum Devices *Vacuum* 47 (6–8) 1996: pp. 771 – 777.

6. **Alghoul, M. A., Sulaiman, M. Y., Azmi, B. Z., et al.** Review of Materials for Solar Thermal Collectors *Anti-Corrosion Methods and Materials* 52 (4) 2005: pp. 199 – 206.
7. **Giedraitis, A., Tamulevičius, S., Gudaitis, R., et al.** Optical Transmittance Method for In-situ Analysis of Adsorption Phenomena from Residual Gases *Materials Science* (*Medžiagotyra*) 13 (4) 2007: pp.351 – 354.
8. Gas-doped Getters for b/w CRT-s *Catalogue from SAES Getters Concern Milan*, Italy, 1970.
9. TYC-getters for Antenna Mounting in Colour CRT-s *Catalogue from SAES Getters Concern* Milan, Italy, 1969.
10. **Cullity, B. D.** Elements of X-ray Diffraction. 2nd ed., Addition-Wesley, Massachusetts, 1978: p. 102.
11. **Impoco, G., Carrato, S., Caccamo, M. L., et al.** Quantitative Analysis of Cheese Microstructure Using SEM Imagery *In: Communications of SIMAI (Società Italiana di Matematica Applicata e Industriale) Congress* vol. 2 2006: pp. 1 – 4.
12. Research Services Branch NIMH & NINDS. ImageJ – Image Processing and Analysis in Java. Web site: http://rsb.info.nih.gov/ij/.
13. Technical Specification of Evaporable Getter ST15A/15KLS/150 WS5, *SAES Getters*, 2001: p. 1.
14. Technical Specification of evaporable Getter ST15/20KLS/200 VS 110°, *SAES Getters*, 1993: p. 1.
15. **Sciuccati, F., Mazzeri, G. C., Ferrario, B.** A Study of the Residual Gas Atmosphere During Operational Life of 20" 110° CCRTs as a Function of Bake-out Temperature During Processing *Vacuum* 38 (8 – 10) 1988: pp. 847 – 51.
16. ASTM Subcommittee F04.16. F1877-98. Standard Practice for Characterization of Particles. In: 2000 Medical Devices and Services. 2000, American Society for Testing and Materials, West Conshohocken, PA. p. 1582.
17. **Goswami, A.** Thin Film Fundamentals. New Age International Publishers, New Delhi, 1996.
18. **Wagner, C. D., Riggs, W. M., Davis, L. E., Moulder, J. F.** Handbook of X-ray Photoelectron Spectroscopy. Perkin-Elmer Corporation, 1978: 190 p.
19. **Charles, D., et al.** NIST Standard Reference Database 20, Version 3.4 NIST X-ray Photoelectron Spectroscopy Database, Version 3.5 (National Institute of Standards and Technology, Gaithersburg, 2003); Web site: http://srdata.nist.gov/xps/.
20. **Perdijk, H. J. R.** A Compilation of Gas Reactions as Observed in Electron Tubes *Vacuum* 21 (6) 1971: p. 223.
21. **Verhoeven, J. A. Th., Van Doveren, H.** Interactions of Residual Gases with a Barium Film as Measured by AES and XPS *Journal of Vacuum Science and Technology* 20 (1) 1982: pp. 64 – 74.